

# Spectroscopic and QM/MM investigations of Chloroperoxidase catalyzed degradation of orange G



Rui Zhang <sup>a,1</sup>, Qinghao He <sup>a</sup>, Yi Huang <sup>b</sup>, Xiaotang Wang <sup>a,\*</sup>

<sup>a</sup> Department of Chemistry & Biochemistry, Florida International University, Miami, FL 33199 USA

<sup>b</sup> School of Chemistry and Chemical Engineering, Xianyang Normal University, Xianyang, 712000 China

## ARTICLE INFO

### Article history:

Received 28 September 2015

Received in revised form

5 February 2016

Accepted 24 February 2016

Available online 27 February 2016

### Keywords:

Chloroperoxidase

Heme protein

Compound X

Halide dependent

Biodegradation

Azo dye

## ABSTRACT

Chloroperoxidase (CPO), a heme-thiolate protein, from *Caldariomyces fumago* catalyzes a plethora of reactions including halogenation, dismutation, epoxidation, and oxidation. Although all CPO-catalyzed reactions go through a common intermediate, compound I, different mechanisms are followed in subsequent transformations. To understand the mechanism of CPO-catalyzed halide-dependent degradation of orange G, the role of halide and pH was systematically investigated. It is revealed that formation and protonation of compound X, a long-sought after hypochlorite heme adduct intermediate existed during CPO-catalyzed halide-dependent reactions, significantly lowers the reaction barrier and increases the efficiency of CPO-catalyzed orange G degradation. The extremely acidic optimal reaction pH suggests the protonation of a residue, presumably, Glu 183 in CPO catalysis. Halide dependent studies showed that  $K_{cat}$  is higher in the presence of  $Br^-$  than in the presence of  $Cl^-$ . The degradation products of orange G indicate the cleavage at a single position of orange G, demonstrating a high regioselectivity of CPO-catalyzed degradation. Based on our kinetic, NMR and QM/MM studies, the mechanism of CPO-catalyzed orange G degradation was proposed.

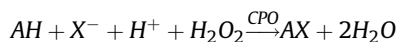
© 2016 Elsevier Inc. All rights reserved.

## 1. Introduction

Chloroperoxidase (CPO), a heme-thiolate protein secreted by *Caldariomyces fumago*, has been the subject of extensive contemporary investigations owing to its versatile catalytic activities. In addition to catalyzing native halogenation reactions involved in the biosynthesis of halogen-containing compounds [1], CPO also catalyzes reactions typical of traditional heme peroxidases [2], catalases [2], and cytochrome P450 enzymes [3–6]. The diversity of CPO catalyzed reactions keeps expanding as more investigations are carried out [7–9]. The dehaloperoxidase activity of CPO has only

been demonstrated recently [10].

Although CPO displays a broad array of catalytic activities, its primary biological function appears to be the halide-dependent halogenation of aliphatic substrates according to the following reaction:



where AH represents an organic acceptor molecule, and  $X^-$  can be any halide ions except  $F^-$  [1]. The pathway for CPO-catalyzed halogenations has been proposed to involve a ferric hypohalite intermediate known as compound X [11–13]. However, the proof of compound X and the exact role of halide ions in CPO-catalyzed reactions have been challenging and warrant further investigations [14,15]. In particular, CPO-catalyzed reactions in the absence or presence of halide are found to proceed with distinct mechanisms. For instance, CPO catalyzed oxidation of sulfides is enantioselective in the absence of chloride, whereas in the presence of chloride this enantioselectivity is diminished [16]. In addition to the well documented broad spectrum of activities, CPO can also oxidatively degrade a number of selected azo dyes [17], a novel activity that may have important environmental

**Abbreviations:** CPO, chloroperoxidase; COSY, correlation spectroscopy; ESP, ElectroStatic Potential; DFT, density function theory; Glu, glutamic acid; His, histidine; HRP, horseradish peroxidase; LPO, Lactoperoxidase; LiP, lignin peroxidase; LC-MS, liquid chromatography–mass spectrometry; MPO, myeloperoxidase; NEB, nudged elastic band; NMR, nuclear magnetic resonance; QM/MM, quantum mechanics/molecular mechanics; Rz, Reinheitszahl value; SPC/E, extended simple point charge.

\* Corresponding author.

E-mail address: [wangx@fiu.edu](mailto:wangx@fiu.edu) (X. Wang).

<sup>1</sup> Present address: Department of Chemistry & Biochemistry, Texas Tech University, Lubbock, TX 79409, USA.

implications.

The widespread use of synthetic dyes in textile, paper, food, and other industries has caused considerable environmental pollution and imposed potential hazards to human health [18–20]. Most synthetic dyes are resistant to degradation under mild conditions, as these dyes are designed with the high chemical and photolytic stability to satisfy their intended applications. Azo dyes, the largest and most versatile class of synthetic dyes that constitutes 60–80% of all organic colorants [18,20,21], are even resistant to microbial attacks. This recalcitrance to biodegradation is partially attributed to the xenobiotic nature of the azo bonds (–N=N–) [22,23]. To effectively degrade dyes, especially azo dyes, much effort has been made on developing physical [18,24], chemical [18,24], and biological treatments [18,24,25]. Alternatively, the use of enzyme is very promising in terms of its environmentally-friendly nature and high degradation efficiency [20,26]. Recently, Jiang's group reported a highly-efficient degradation of azo dyes, orange G and Sunset yellow, using chloroperoxidase (CPO) [17]. CPO is promising in environmental applications as it is stable [27] and remains active under harsh reaction conditions that most other peroxidases would not tolerate or even be denatured [28]. Moreover, CPO can be produced at high yield (up to 1–1.5 g/liter) [29]. Therefore, it is imperative that the details of CPO-catalyzed degradation be fully characterized.

The aim of the present work is to investigate the mechanism of CPO-catalyzed degradation of azo dyes (Scheme 1), particularly orange G, with hydrogen peroxide (H<sub>2</sub>O<sub>2</sub>) in the presence of halide ions (X<sup>–</sup>). The degradation conditions, including pH, chloride/bromide concentrations, and H<sub>2</sub>O<sub>2</sub> concentration were examined and optimized. It was found that in the absence of halide ion the degradation is almost negligible. However, the presence of chloride/bromide ion significantly enhanced the degradation rate and efficiency, indicating the involvement of a halide-containing intermediate (Fe–OX<sup>–</sup>, compound X) during degradation. A QM/MM approach was employed to characterize the electronic structure of compound X and subsequent generation of HClO. Finally, the degradation products of orange G were firmly established by NMR spectroscopy. This work provides, for the first time, both experimental and theoretical evidences of the important role halide plays in CPO-catalyzed degradation of azo dyes.

## 2. Experimental

### 2.1. Enzymes and chemicals

*Caldariomyces fumago* (ATCC number: 16373) was purchased from ATCC (Manassas, VA). CPO was isolated and purified according to published protocols [30,31]. CPO with Reinheitszahl value (Rz,  $A_{398\text{ nm}}/A_{278\text{ nm}}$ ) of 1.3 or higher was used in all experiments. The concentration of CPO was determined by measuring the absorbance at 398 nm using a molar extinction coefficient of 91,200 M<sup>–1</sup>cm<sup>–1</sup> [1]. The stock solution of CPO was concentrated by centrifuging the protein solution in a Centriprep-30 centrifugal filter device.

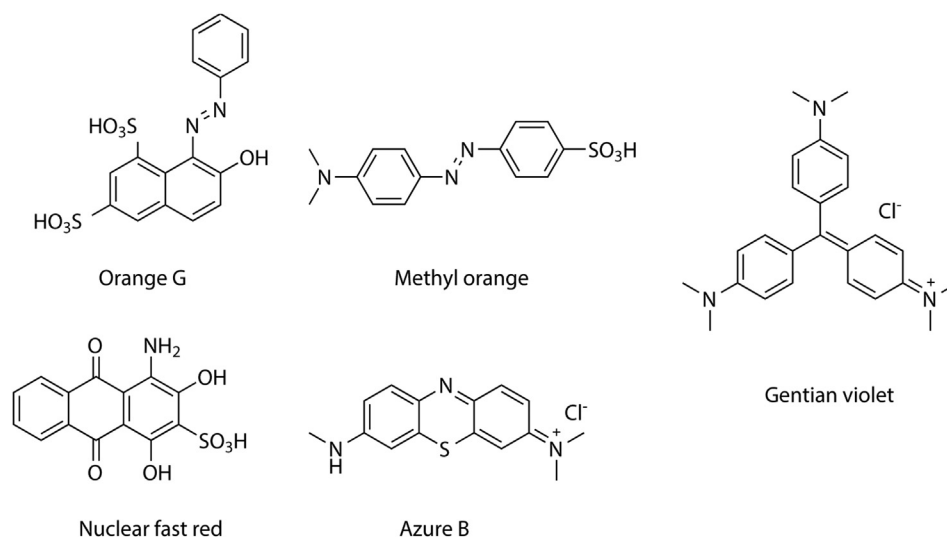
Orange G, methyl orange, and nuclear fast red were purchased from Thermo Fisher Scientific (Waltham, MA). Azure B and gentian violet were obtained from MP Biomedicals (Solon, OH). All other chemicals and solvents were purchased from Sigma-Aldrich (St. Louis, MO). Unless otherwise specified, all dyes used were of biological stain grade and all chemicals were of either reagent or analytical grade. Millipore Milli-Q water (18.2 MΩ) was used throughout.

### 2.2. UV-Vis spectroscopic measurement

UV-Vis spectra were recorded on a CaryBio-300 UV-Vis spectrophotometer. The degradation efficiency was calculated using Equation (1), where  $A_0$  is the absorbance of the dye monitored at the wavelength of maximum absorbance ( $\lambda_{\text{max}}$ ) before addition of H<sub>2</sub>O<sub>2</sub>, and  $A_t$  is the absorbance when it reaches a stable value after addition of H<sub>2</sub>O<sub>2</sub>.

$$\text{Efficiency}(\%) = \frac{A_0 - A_t}{A_0} \times 100 \quad (1)$$

To determine the rate of orange G degradation, the absorbance at 477 nm ( $\lambda_{\text{max}}$ ) was monitored. The rate was calculated according to Equation (2), where  $A_0$  is the absorbance monitored at time  $t_0$ ,  $A_t$  is the absorbance monitored at time  $t_t$ , and 20.7 (mM<sup>–1</sup> cm<sup>–1</sup>) is the reported extinction coefficient of orange G at 477 nm [32].



**Scheme 1.** Structures of synthetic dyes used in this work: orange G (7-hydroxy-8-[(E)-2-phenyldiazen-1-yl]naphthalene-1,3-disulfonic acid), methyl orange (4-[(E)-2-[4-(dimethylamino)phenyl]diazen-1-yl]benzene-1-sulfonic acid), nuclear fast red (1,3-dihydroxy-4-methyl-9,10-dioxo-9,10-dihydroanthracene-2-sulfonic acid), Azure B (3-(dimethylamino)-7-(methylamino)phenothiazin-5-ium chloride), and Gentian violet (Tris(4-(dimethylamino)phenyl)methylium chloride).

$$\text{Rate}(\mu\text{M}/\text{s}) = \frac{A_0 - A_t}{20.7 \times (t_0 - t_t)} \times 1000 \quad (2)$$

Assuming that the reaction follows the Michaelis–Menten kinetics, Michaelis constant ( $K_m$ ) and maximum rate ( $V_{\max}$ ) were obtained from Lineweaver–Burk plot Equation (3), where  $S$  is the concentration of orange G,  $V$  is the initial reaction rate measured in the linear range of degradation (5–10 s).

$$\frac{1}{V} = \frac{K_m}{V_{\max}} \cdot \frac{1}{[S]} + \frac{1}{V_{\max}} \quad (3)$$

The turnover number,  $k_{\text{cat}}$ , was calculated according to Equation (4), where  $E_0$  is the concentration of CPO.

$$V_{\max} = k_{\text{cat}}[E_0] \quad (4)$$

### 2.3. NMR characterization of degradation products from orange G

The NMR experiments were carried out on a Bruker 600 MHz NMR spectrometer operating at a proton frequency of 599.73 MHz. All spectra were recorded at 300 K and two-dimensional data were processed using NMRPipe [33]. The COSY experiment was performed using the standard Bruker pulse sequence (cosyprqf) with 4096 data points in the F2 dimension, and 512 increments in F1. The data was processed to give a matrix of 2048 × 512 points, and a sine bell apodization was applied before Fourier transformation. Chemical shift values were referenced to the residual HDO signal at 4.76 ppm.

### 2.4. QM/MM study on the formation of HClO by compound X

The starting structure for CPO was taken from the high resolution X-ray structure (PDB entry 2CIW). The cyanide ligand in the heme center was manually replaced by  $\text{ClO}^-$  ligand. The structure was solvated in a truncated octahedron box (82 Å) of extended simple point charge (SPC/E) waters. A total of 7624 waters were contained in the system. The protonation states of the titratable amino acid residues of CPO were assigned as follows: +1 for His and Lys, and neutral for Tyr, Glu and Asp. Therefore, the protein has a net charge of +20, thus 20  $\text{Cl}^-$  counter-ions were added to create a neutral system for simulation.

The hybrid quantum mechanics/molecular mechanics (QM/MM) calculations were performed using software NWChem [34], version 6.3. The overall algorithm involves alternating optimizations of QM and MM regions until convergence is achieved. The QM region consisted of heme ligated with sulfur atom (representing cysteine 29) as well as the side chain functional groups of His 105 and Glu 183. The substituents of the heme were not included to simplify calculation. This simplification used in DFT calculations is made as the compound I geometries do not vary noticeably with varying QM region sizes [35]. The covalent bonds crossing to the MM region were capped with hydrogen atoms. The DFT geometry optimizations were performed at the spin-unrestricted B3LYP [36,37] level with LACVP basis sets (LANL2DZ [38] effective core on iron and 6-31G [39] on other atoms). The single point energy calculation was performed at the spin-unrestricted B3LYP with LANL2DZ on iron atom and 6-31 +  $G^*$  on other atoms. The remainder of the protein (MM region) was described at the molecular mechanics level using an AMBER95 force field [40]. During optimization of MM regions, the electrostatic potential (ESP) charges for QM region was calculated and used to compute electrostatic interactions with the MM regions. The initial guess for

transition state was generated using nudged elastic band (NEB) approach [41] implemented in NWChem. The NEB approach optimizes the trial reaction pathway and a total of 10 beads were used for pathway representation.

### 2.5. Molecular docking

Molecular docking of orange G was performed with AutoDock [42], version 4.2.3 to predict the possible binding sites. The structure of CPO for docking was taken from the high resolution X-ray structure (PDB entry 2CIW). Minor modification of X-ray structure was introduced to simplify docking as described previously [43], i.e., glycosylation sites, manganese ion, and crystallographic water in the PDB file were removed.

The orange G structures was built by MarvinSketch, version 6.2, in the JChem software package (ChemAxon, Ltd.) and further optimized with ORCA [44], version 2.9, using density function theory (DFT) with B3LYP//6-31G\*. AutoDockTools [45], version 1.5.4, was used to add Gasteiger charges to CPO (+1.00 was added manually on Fe) and orange G. During simulation, CPO structure was kept rigid. Orange G was simulated in a box centered at the heme iron, which was confined using a grid size of 30 Å × 30 Å × 30 Å with 0.375 Å spacing. Docking consisting of 60 separate simulation runs was performed with 25 million energy evaluations per run.

## 3. Results and discussion

### 3.1. UV-Vis study of CPO-catalyzed degradation of orange G

UV-Vis spectra of orange G (0.01 mM) were recorded in the presence of 0.01 μM CPO, 20 mM chloride ion ( $\text{Cl}^-$ ), and 0.5 mM hydrogen peroxide at pH 2.7. Fig. 1A illustrates the typical UV-Vis spectra of orange G obtained during the degradation process. Before addition of hydrogen peroxide ( $\text{H}_2\text{O}_2$ ), the spectrum of orange G showed a strong absorption at 477 nm ( $\lambda_{\text{max}}$ ) with a shoulder at 419 nm (Fig. 1A, black line). These absorption bands originate from the azo bond ( $-\text{N}=\text{N}-$ ) of orange G that undergoes azo-hydrazone tautomerization [46]. The weak absorption at 329 nm (Fig. 1A, black line) is due to the  $\pi$  to  $\pi^*$  transition in the naphthalene structure [47]. Five minutes after addition of  $\text{H}_2\text{O}_2$ , the absorption at 477 nm significantly decreased (Fig. 1A, red line), indicating the cleavage of orange G. Essentially identical spectral changes were observed after hypochlorous acid (HClO) alone was added to orange G (Fig. 1A, blue line), indicating the formation of similar products as in the CPO- $\text{H}_2\text{O}_2$ - $\text{Cl}^-$  system. It is worth mentioning that degradation of orange G is negligible in the presence of CPO and  $\text{H}_2\text{O}_2$  without  $\text{Cl}^-$  (Fig. 1A, yellow line), suggesting the imperative role of  $\text{Cl}^-$  in CPO-catalyzed degradation of azo dyes.

Fig. 1B shows the kinetic behavior of orange G at 477 nm during CPO-catalyzed degradation. After addition of  $\text{H}_2\text{O}_2$ , the absorbance of orange G decreased continuously and approached baseline in approximately 70 s (Fig. 1B), indicating a fast and efficient degradation. The degradation rate was calculated to be 21 in the first 10 s, 30 between 10 and 30 s, and 4 μmole substrate/s per micro-mole of CPO between 30 and 70 s. The decrease of the absorbance was linear within a short period after reaction is initiated (10–30 s) (Fig. 1B, inset). Thus, the reaction rate was calculated within this linear range and discussed below unless otherwise specified.

Table 1 lists the degradation efficiency of a variety of synthetic dyes including orange G, methyl orange, nuclear fast red, gentian violet, and azure B in the CPO- $\text{H}_2\text{O}_2$ - $\text{Cl}^-$  system. The degradation of all dyes (0.01 mM) proceeded with high efficiency (70.4–99% within 180 s). This result demonstrates that the CPO- $\text{H}_2\text{O}_2$ - $\text{Cl}^-$  system is highly efficient to degrade different types of synthetic

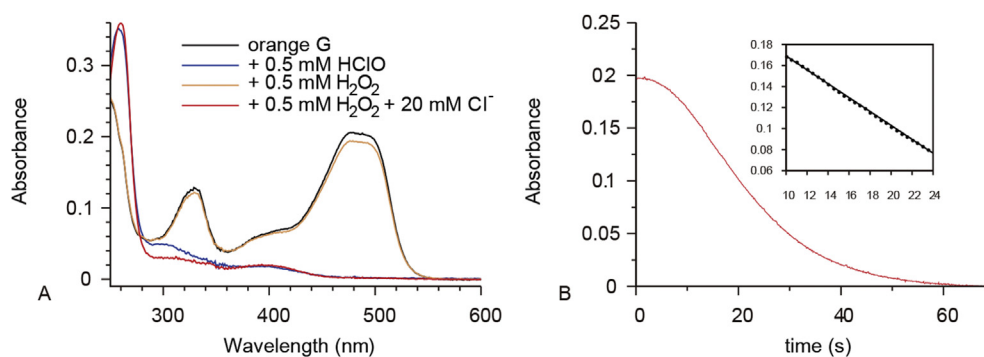


**Fig. 1.** UV-Vis spectra of 0.01 mM orange G (A, black trace), and in the presence of 0.5 mM  $\text{H}_2\text{O}_2$  (yellow trace), 0.5 mM  $\text{H}_2\text{O}_2$  and 20 mM  $\text{Cl}^-$  (red trace), and 0.5 mM  $\text{HClO}$  only (blue trace). (B) Changes of absorbance at 477 nm in the presence of 20 mM  $\text{Cl}^-$  and 0.5 mM  $\text{H}_2\text{O}_2$ . All spectra were obtained in 3 ml phosphate buffer (50 mM, pH 2.7) containing 0.01  $\mu\text{M}$  CPO. (For interpretation of the references to colour in this figure legend, the reader is referred to the web version of this article).

**Table 1**  
Degradation efficiency of selected synthetic dyes in CPO- $\text{H}_2\text{O}_2$ - $\text{Cl}^-$  system.

Dye	$\lambda_{\text{max}}$ (nm)	Time (s)	Efficiency <sup>a,b</sup>
Orange G	477	<80	99.3 $\pm$ 1.2%
Methyl orange	506	<10	98.1 $\pm$ 5.7%
Gentian violet	593	<40	96.5 $\pm$ 0.8%
Nuclear fast red	518	<5	96.7 $\pm$ 3.1%
Azure B	648	<180	70.4 $\pm$ 2.2%

<sup>a</sup> The degradation time and efficiency of dyes were evaluated from the visible absorbance at  $\lambda_{\text{max}}$ .

<sup>b</sup> Reaction condition: 50 mM phosphate buffer (pH = 2.7) containing 10  $\mu\text{M}$  synthetic dyes, 0.01  $\mu\text{M}$  CPO, and 20 mM  $\text{Cl}^-$ , and a final concentration of 0.5 mM  $\text{H}_2\text{O}_2$ , at 20 °C.

dyes, suggesting the potential of utilizing CPO in large-scale degradation of these compounds in environmental protection and waste management.

### 3.2. The effect of chloride and bromide on the degradation of orange G

To examine the effect of chloride ( $\text{Cl}^-$ ) and bromide ( $\text{Br}^-$ ) on the degradation of azo dyes, the rate of orange G degradation was measured in the presence of varying concentrations of  $\text{Cl}^-$  or  $\text{Br}^-$  (0–100 mM). Fig. 2A shows the relationship between rate of orange G degradation and the concentration of  $\text{Cl}^-/\text{Br}^-$ . As the concentration of  $\text{Cl}^-$  increased from 0 to 20 mM, the degradation rate increased 400-fold from 0.075 to 30  $\mu\text{mole substrate/s}$  per micromole of CPO (Fig. 2A). This observation suggests that  $\text{Cl}^-$  (or  $\text{Br}^-$ ) participates in the degradation of orange G, presumably via formation of  $\text{HClO}$ . The formation of this powerful oxidizing/

chlorinating agent in the presence of  $\text{Cl}^-$  and  $\text{H}_2\text{O}_2$  has also been reported for myeloperoxidase (MPO) [48–50]. It should be noted that the rate of degradation gradually decreased down to ~30% of the maximum, as the concentration of chloride was further increased from 20 to 100 mM, (Fig. 2A). This may be attributed to the formation of molecular chlorine ( $\text{Cl}_2$ ) between  $\text{HClO}$  and the excess amount of  $\text{Cl}^-$ , lowering the concentration of  $\text{HClO}$  available for the degradation of orange G [51].

To prove the involvement of  $\text{HClO}/\text{HBrO}$  in the degradation of orange G, the rate constant of the direct reaction between hypochlorous acid/hypobromous acid (10  $\mu\text{M}$ ) and Orange G (10  $\mu\text{M}$ ) was measured in a pH dependent manner. As shown in Fig. S1, the rate of degradation showed a similar pH dependent pattern as were observed for the CPO- $\text{H}_2\text{O}_2$ - $\text{Cl}^-$  and CPO- $\text{H}_2\text{O}_2$ - $\text{Br}^-$  systems. This supports our hypothesis that  $\text{HClO}/\text{HBrO}$  was formed during CPO catalyzed orange G degradation. To further confirm the formation of  $\text{HClO}$  or  $\text{HBrO}$  in CPO catalyzed halide-dependent degradation of orange G, taurine, a  $\text{HClO}/\text{HBrO}$  trap, was added to both the CPO- $\text{H}_2\text{O}_2$ - $\text{Cl}^-$  and CPO- $\text{H}_2\text{O}_2$ - $\text{Br}^-$  systems as well as the direct reaction of hypochlorous acid and hypobromous acid with Orange G. As expected, taurine significantly decreased the rate of Orange G degradation by hypochlorous or hypobromous acid. However, to our surprise, no obvious effect of taurine on the rate of CPO catalyzed orange G degradation was observed. This is in agreement with the hypothesis that the  $\text{HClO}/\text{HBrO}$  formed in the CPO system reacted with orange G before they were released to solution [14,52]. This also supports our docking study that suggests the binding of orange G within the wide channel of CPO (data not shown).

Table 2 lists the Michaelis constant ( $K_m$ ) and the turnover number ( $k_{\text{cat}}$ ) obtained in the presence of  $\text{Cl}^-/\text{Br}^-$ . These values are

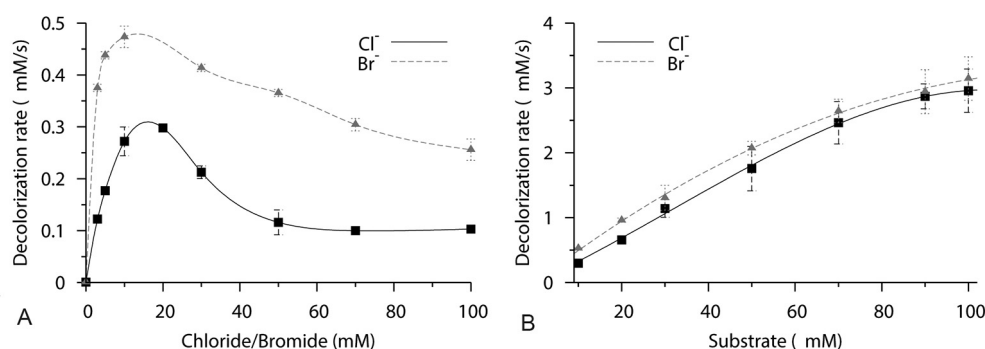


**Fig. 2.** The effect of chloride (A, rectangle), bromide (A, triangle) and substrate (B) concentration on degradation of orange G. Data were obtained from triplicate experiments in 50 mM phosphate buffer (pH 2.7) containing 0.01  $\mu\text{M}$  CPO and a final concentration of 0.5 mM  $\text{H}_2\text{O}_2$  with a fixed concentration of 10  $\mu\text{M}$  orange G (A) or 20 mM  $\text{Cl}^-/\text{Br}^-$  (B).

**Table 2**  
Kinetic parameters of orange G degradation catalyzed by CPO.<sup>a</sup>

	$K_m$ ( $\mu\text{M}$ )	$V_m$ ( $\mu\text{M}$ )	$k_{\text{cat}}$ ( $\text{s}^{-1}$ )	$k_{\text{cat}}/K_m$ ( $\mu\text{M}^{-1}\text{s}^{-1}$ )	$R^2$
$\text{Cl}^-$	174	9.12	911	5.24	0.989
$\text{Br}^-$	131	7.40	740	5.65	0.994

<sup>a</sup> The parameters were obtained in 50 mM phosphate buffer (pH 2.7) containing 0.01–0.1 mM orange G, 0.01  $\mu\text{M}$  CPO, 20 mM  $\text{Cl}^-/\text{Br}^-$  and a final concentration of 0.5 mM  $\text{H}_2\text{O}_2$ , at 20 °C.

consistent in magnitude with those reported by Zhang et al. [17]. It was found that the  $K_m$  obtained in the presence of  $\text{Br}^-$  is lower than that in the presence of  $\text{Cl}^-$ . On the other hand, the  $k_{\text{cat}}$  in the presence of  $\text{Cl}^-$  is higher than that in the presence of  $\text{Br}^-$ . The overall rates of orange G degradation in the presence of  $\text{Br}^-$  are much higher than that in the presence of  $\text{Cl}^-$  (Fig. 2B), suggesting that either  $\text{HBrO}$  is produced more efficiently than  $\text{HClO}$  or  $\text{HBrO}$  is more powerful than  $\text{HClO}$  in degrading orange G within CPO environment. The high degradation rate in the presence of  $\text{Br}^-$  is consistent with the relative rates of CPO-catalyzed halogenation, i.e.,  $\text{Br}^- > \text{Cl}^-$  [53], which were rationalized by the relative rates of the nucleophilic attack of halide ion on compound I [51]. In addition, the high rate of  $\text{Br}^-$ -assisted degradation could also be attributed to the fact that the dissociation constant of CPO-bromide complex is higher than that of CPO-chloride complex [54]. Although chloride binding site was not found in the crystal structure of CPO at pH 6.0 [55], multiple bromide binding sites were identified at the active site of CPO [56]. Nevertheless, chloride ion was reported to be responsible for the formation of the short-lived halogenating intermediate in CPO catalyzed halogenation reactions [57]. Our results demonstrate that halide binding to CPO is an essential step in the degradation of azo dyes, in agreement with crystal structural analysis [55,56].

### 3.3. The effect of pH

To probe the effect of pH on CPO catalyzed orange G degradation, the reaction rate and efficiency were determined in the pH range of 2.7–5.0. In the presence of 20 mM  $\text{Cl}^-$ , the degradation rate gradually decreased as pH was increased from 2.7 to 5.0 (Fig. 3A). This could be attributed to changes in the protonation state of the ionizable group involved in  $\text{Cl}^-$  binding at different pH [54]. This pH dependence also indicates that the protonation of the enzyme-activated  $\text{ClO}^-$  (to  $\text{HClO}$ ), compound X, is a prerequisite for orange G degradation. This complies with a previous report that heme- $\text{HClO}$  complex catalyzed the chlorination of monochlorodimedone, whereas the corresponding heme- $\text{ClO}^-$  complex

was unreactive [58].

The results shown in Fig. 3 demonstrated that in the presence of 20 mM  $\text{Cl}^-$ , the optimum pH for the degradation of orange G is 2.7, identical to the optimum pH for CPO-catalyzed halogenation [59]. The fact that CPO-catalyzed dye degradation and halogenation optimize at the same pH and halide concentration implicates the involvement of common intermediates such as compound I and compound X, and thus have an identical mechanism. The degradation efficiency decreased as pH reaches 5.0 (Fig. 3B). Complete degradation took approximately an hour at this pH. This is consistent with the observed decrease in degradation rate at elevated pH (Fig. 3A).

### 3.4. Effect of hydrogen peroxide concentration

To examine the effect of  $\text{H}_2\text{O}_2$  concentration on the degradation of azo dyes, the degradation rate of orange G (0.01 mM) was determined in the presence of varying concentrations of  $\text{H}_2\text{O}_2$  (0.1–5.0 mM). As expected, the degradation rate is greatly enhanced as the concentration of  $\text{H}_2\text{O}_2$  increased up to 0.5 mM (Fig. S2). However, further increasing  $\text{H}_2\text{O}_2$  concentration (from 0.5 to 5.0 mM) decreases the degradation rate. This could be attributed to the fact that excess  $\text{H}_2\text{O}_2$  would compete with  $\text{Cl}^-$  for compound I [60,61]. It is also possible that CPO is inactivated at high concentrations of  $\text{H}_2\text{O}_2$  due to formation of a highly reactive iron peroxy species (compound III) that leads to heme degradation [62]. Nevertheless, CPO is still a stable enzyme in the presence of  $\text{H}_2\text{O}_2$ , as its half-life time is reported to be at least five-fold higher than that of other peroxidases such as horseradish peroxidase (HRP), lignin peroxidase (LiP), and lactoperoxidase (LPO) [63].

### 3.5. Products from CPO-catalyzed orange G degradation

Proton NMR spectra of orange G (1.0 mM) and its degradation products were shown in Fig. 4. With addition of  $\text{H}_2\text{O}_2$ , orange G signals (Fig. 4A) disappeared with concomitant appearance of new signals from cleavage products (Fig. 4B). Theoretically, cleavage can take place at multiple positions [64]. However, CPO catalyzed cleavage took place at only one position, demonstrating a strict regioselectivity of CPO. Six hours after addition of  $\text{H}_2\text{O}_2$ , peaks m (7.96 ppm), p (8.28 ppm), and o (8.55 ppm) shown in Fig. 4 B disappeared with three new peaks o (6.92 ppm), p (6.98 ppm), and m (7.31 ppm) emerged as shown in Fig. 4C. The chemical shifts and splitting pattern of these new peaks suggest the formation of phenol from orange G degradation. This was further confirmed by comparison of the NMR spectrum of the degradation product with that of authentic phenol at pH 2.7 (Fig. S3).

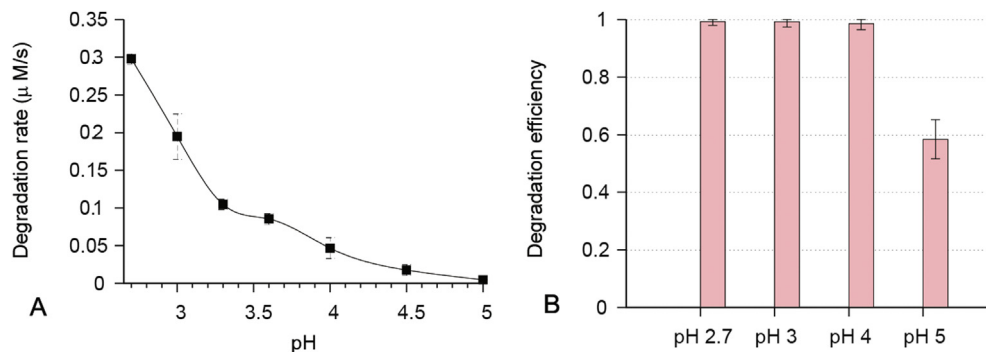


**Fig. 3.** pH dependence of orange G (10  $\mu\text{M}$ ) degradation. (A) The degradation rate of orange G in the presence of 20 mM  $\text{Cl}^-$  as a function of pH. (B) The degradation efficiency of orange G in the presence of 20 mM  $\text{Cl}^-$  in the pH range of 2.7–5.0. The data were obtained from triplicate experiments in 50 mM phosphate buffer containing 0.01  $\mu\text{M}$  CPO and a final concentration of 0.5 mM  $\text{H}_2\text{O}_2$ .

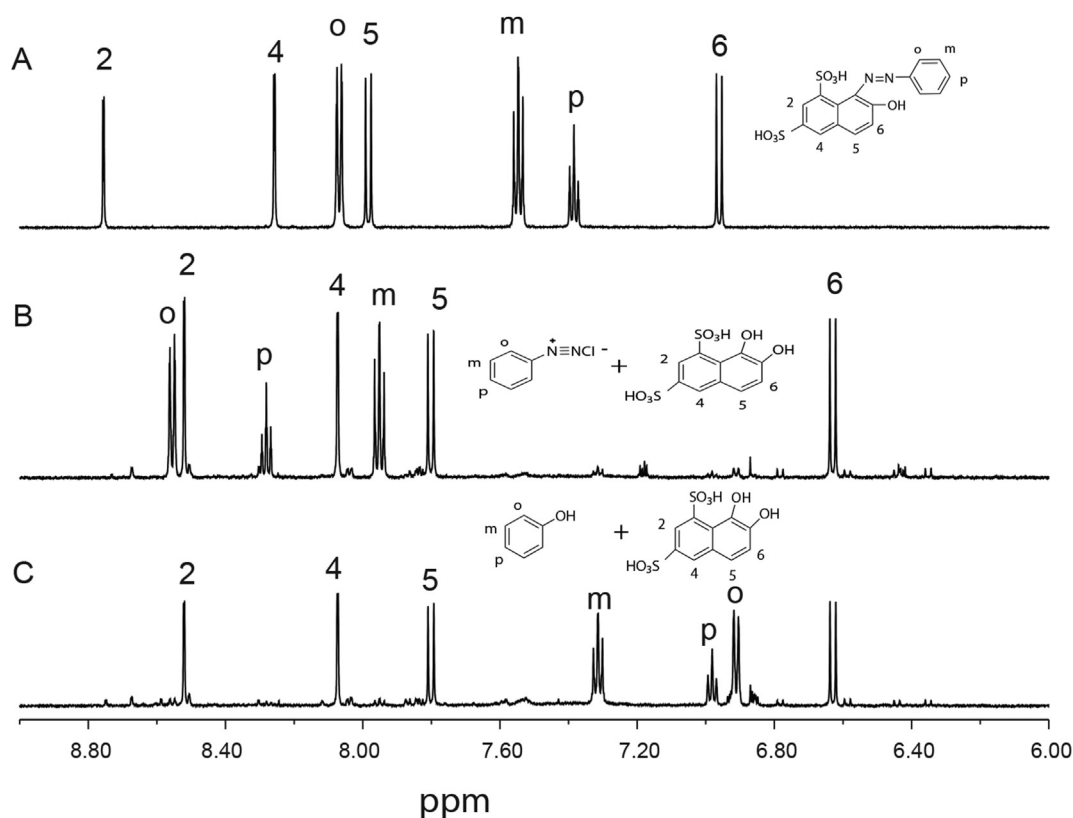


**Fig. 4.** Proton NMR spectra of orange G (1.0 mM) and its degradation products. The NMR sample of orange G (1.0 mM) was prepared in 50 mM deuterated phosphate buffer containing 2.0  $\mu$ M CPO and 20 mM  $\text{Cl}^-$  at pH 2.7 (A) without and (B) with the addition of a final concentration of 4 mM  $\text{H}_2\text{O}_2$ . (C) The same tested solution of (B) was measured 6 h after the initial addition of  $\text{H}_2\text{O}_2$ . Herein, DCl solution (1.0 M) prepared from the dilution of DCl (35% wt.% in  $\text{D}_2\text{O}$ ) with  $\text{D}_2\text{O}$  was used to adjust pH. To minimize residual solvent peaks,  $\text{H}_2\text{O}_2$  solution (0.1 M) prepared from the dilution of  $\text{H}_2\text{O}_2$  (35% wt.% in  $\text{H}_2\text{O}$ ) with  $\text{D}_2\text{O}$  was used to initiate reactions, and CPO stock solution (final 1.0  $\mu$ M) was added before and then after additional of  $\text{H}_2\text{O}_2$  to better complete degradation.

To confirm the identity of products from orange G degradation, two-dimensional  $^1\text{H}$ – $^1\text{H}$  NMR correlation spectrum was recorded (Fig. S4). The peaks at 7.96, 8.28, and 8.55 ppm are strongly correlated, indicating that the corresponding protons are on the same aromatic ring. The correlation (Fig. S4) and splitting pattern (Fig. 4B) of these peaks suggest the formation of benzene diazonium in the initial degradation of orange G. It has been demonstrated that benzene diazonium is unstable and undergoes further decomposition [65]. The disappearance of benzene diazonium signals with time proves the transient nature of this compound that is further converted to the final product phenol, which shows correlations at 6.92, 6.98, and 7.31 ppm (Fig. S4). Formation of phenol from orange G degradation have been reported by Madhavan et al. [66]. Two peaks at 7.79 and 6.64 ppm are assigned to 5- and 6- protons of 7,8-dihydroxynaphthalene-1,3-disulfonic acid based on their strong correlation and the splitting pattern. Formation of 7,8-dihydroxynaphthalene-1,3-disulfonic acid from orange G degradation has been demonstrated in several studies [66]. This is further confirmed by the weak correlation between peaks at 8.07 and 8.52 due to long range coupling between 2- and 4- protons of the benzene ring bearing 1,3-sulfonate groups. To our surprise, halogenated compounds, such as chlorophenols, were not found in the CPO- $\text{H}_2\text{O}_2$ - $\text{Cl}^-$  system. This is consistent with the degradation products determined by liquid chromatography–mass spectrometry (LC-MS) [17]. The absence of halogenated products is often desirable since the toxicity of chlorophenols may constitute additional environmental considerations [67,68].

### 3.6. QM/MM study of compound X and HClO generation

Compound X, a ferric hypochlorite adduct, has long been proposed as an important intermediate in enzymatic halogenation [11,69]. The existence of compound X is supported by the steady-state kinetics of chlorination reactions [70]. However, compound X has a very transient existence [70], making it difficult to characterize the structural features and the mechanistic role of this intermediate. To characterize the formation of compound X and its role in orange G degradation, a QM/MM model of compound X was built (Fig. 5A). The structure of CPO compound X has never been addressed before, while the electronic structure of CPO compound I and compound II have been extensively studied by QM/MM and well established [35,71–73]. We found that the structure of compound X resembles that of compound II. For instance, the Fe–O bond distance is found to be 1.81 Å for compound X (Table 3), essentially identical to that reported for CPO compound II (1.82 Å, 1.81 Å from DFT) [74]. In contrast, for compound I, this distance was relatively short (only 1.62 Å) as calculated by DFT [74]. Compound II is reported to be a protonated ferryl adduct (Fe-(OH)), in which the protonation of oxoiron (IV) lowers the Fe–O bond order compared to compound I [74]. Clearly, the Fe–O bond distance of compound X is affected by chloride binding to oxoiron (Fe–OCl). It is also worth mentioning that compound II is the second intermediate following compound I in halide independent oxidation reaction mechanism, while compound X is the second intermediate following compound I in halide dependent reactions such as chlorination reactions. Hence, the structural similarity between compound X and compound II may explain the diverse catalytic activity of CPO. On the

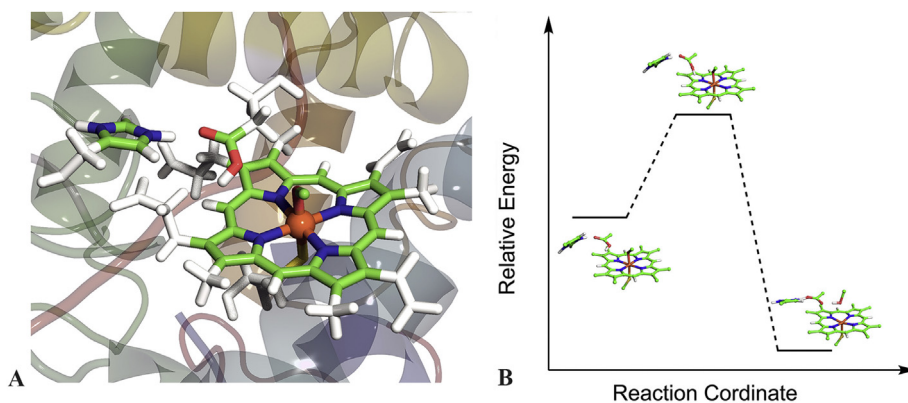


**Fig. 5.** The QM/MM model of CPO compound X. (A) Ribbon and stick representations of the structure of compound X optimized by QM/MM. The QM region is shown in color, while the linked MM region is shown in white. (B) The energy profile of QM/MM calculated compound X, transition state, and CPO complexed with HClO. Only the QM regions including heme, side chains of C29, H105, and E183 (with hydrogen as link atom) are shown for the sake of clarity.

**Table 3**

Geometrical parameters of compound X, transition state, and CPO complexed with HClO.

	Compound X	Transition state, Fe(IV)	CPO/HClO, Fe(III)
Bond (Å)			
Fe–O	1.81	1.81	3.70
Fe–S	2.45	2.42	2.45
O–Cl	1.83	1.84	1.85
O–H	3.92	3.16	1.03
O <sub>E183</sub> –H <sub>H105</sub>	1.63	1.55	1.34
N <sub>H105</sub> –H <sub>H105</sub>	1.05	1.06	1.18
O <sub>E183</sub> –N <sub>H105</sub>	2.66	2.61	2.50
Angle			
H–O–Cl	64.78	66.32	104.76

other hand, the Fe–S distance is found to be 2.45 Å for compound X (Table 3), and 2.48 Å (and 2.6 Å from DFT) for compound I and 2.40 Å (and 2.39 Å from DFT) in compound II [72,74]. The change of Fe–S bond distance may be driven by different interactions between the proximal thiolate and the distal oxygen ligand (i.e., H<sub>2</sub>O, OH<sup>−</sup>, and ClO<sup>−</sup>).

There is a hydrogen transfer from Glu 183 to ferryl oxygen during conversion of compound X to the resting state of CPO (Fig. 5B), since the addition of hydrogen to Fe–OCl<sup>−</sup> is necessary for the release of HClO. To ensure this hydrogen transfer, Glu 183, the only polar group close to oxoiron that can function as an acid-base catalyst in the active site [55], has to be protonated. This also explains the extremely acidic optimum pH for CPO catalyzed Cl<sup>−</sup> dependent reactions. The hydrogen transfer is made possible by conformational changes of the protein during the course of catalysis [43,55,75,76]. Significantly, the O–H distance of Glu 183 and His 105 decreases from 1.63 Å to 1.34 Å (Table 3) as compound X is converted to CPO–HClO complex, while the corresponding N–H distance of His 105 increased from 1.05 Å to 1.18 Å, indicating a sharing of the proton between Glu 183 and His 105. Moreover, the O–N distance of Glu 183 and His105 decreased from 2.66 Å to 2.50 Å. These conformational changes may help to hold Glu183 in an appropriate place and orientation to facilitate the hydrogen transfer from Glu 183 to the iron bound ClO<sup>−</sup>, leading to the formation of HClO. This is consistent with the observation that substitution of Glu 183 with a His is detrimental to CPO's chlorination activity [77].

In the final state, HClO is formed and released from the heme. The release of HClO substantially lowers the quantum energy of compound X by 130 kJ/mol (Table S1), while the reaction barrier for

compound X to the transition state is 100 kJ/mol. Hence, HClO generation decreases the reaction energy barrier and drives the chlorination reaction forward (Fig. 5B).

### 3.7. Mechanism of CPO-catalyzed orange G degradation

On the basis of NMR, QM/MM, and UV-Vis spectroscopic studies, a mechanism of CPO-catalyzed degradation of orange G is proposed (Fig. 6). As for all CPO-catalyzed reactions, the ferric state of CPO (1) reacts with an equivalent of H<sub>2</sub>O<sub>2</sub> to produce an oxoferryl π-cation radical intermediate (Fe=O<sup>+</sup>, (2)), compound I [78,79]. Rather than extracting an electron from an organic substrate in most peroxidase type reactions, CPO compound I captures Cl<sup>−</sup> or Br<sup>−</sup> [80], and forms a hypochlorite adduct (Fe–OX<sup>−</sup>, (3)), compound X [11]. The different binding affinity of Cl<sup>−</sup> or Br<sup>−</sup> to CPO may account for the distinct degradation rate of orange G in the presence of Cl<sup>−</sup>/Br<sup>−</sup> (Fig. 2). In acidic environment, compound X is protonated to form hypochlorous/hypobromous acid (HClO/HBrO). For halogenation reaction, the formation of HClO (or HBrO) is very likely, as it was reported that the presence of HClO reduced reaction barrier of keto-enol tautomerization of beta-cyclopentanedione by 18.8 kJ/mol relative to the gas phase [69]. The hypothesis of protonation of compound X is further supported by our pH dependence experiments in this work. Alternatively, HClO/HBrO may be trapped within the active-site of CPO, as several studies have suggested that CPO chlorinating intermediate cannot escape from the active-site [14,52]. Although our docking study suggests that orange G is unfavorably located in the active site, probably due to steric hindrance, orange G is able to bind in the wide channel that connects the protein surface with the heme (data not shown). Consequently, the trapped HClO/HBrO forms chlorinium/bromonium ion (Cl<sup>+</sup>/Br<sup>+</sup>) that breaks the C–N bond of orange G, meanwhile the ferric resting state of CPO is regenerated. The formation of Cl<sup>+</sup> from HClO has been demonstrated in free solution [81,82] and in myeloperoxidase-catalyzed reactions [83].

The cleavage of orange G (5) occurs exclusively between the naphthalene ring and azo group to produce 7,8-dihydroxynaphthalene-1,3-disulfonic acid (8) and benzene diazonium ion (6) [17]. The diazonium ion (6) formed is further decomposed to phenol (7) by releasing a nitrogen molecule [65]. Although generation of phenols from diazonium salts normally requires heating to approximately 60 °C, under the extremely acidic conditions used in our reaction system, it is possible for the reaction to proceed at noticeable rate at room temperature [84].

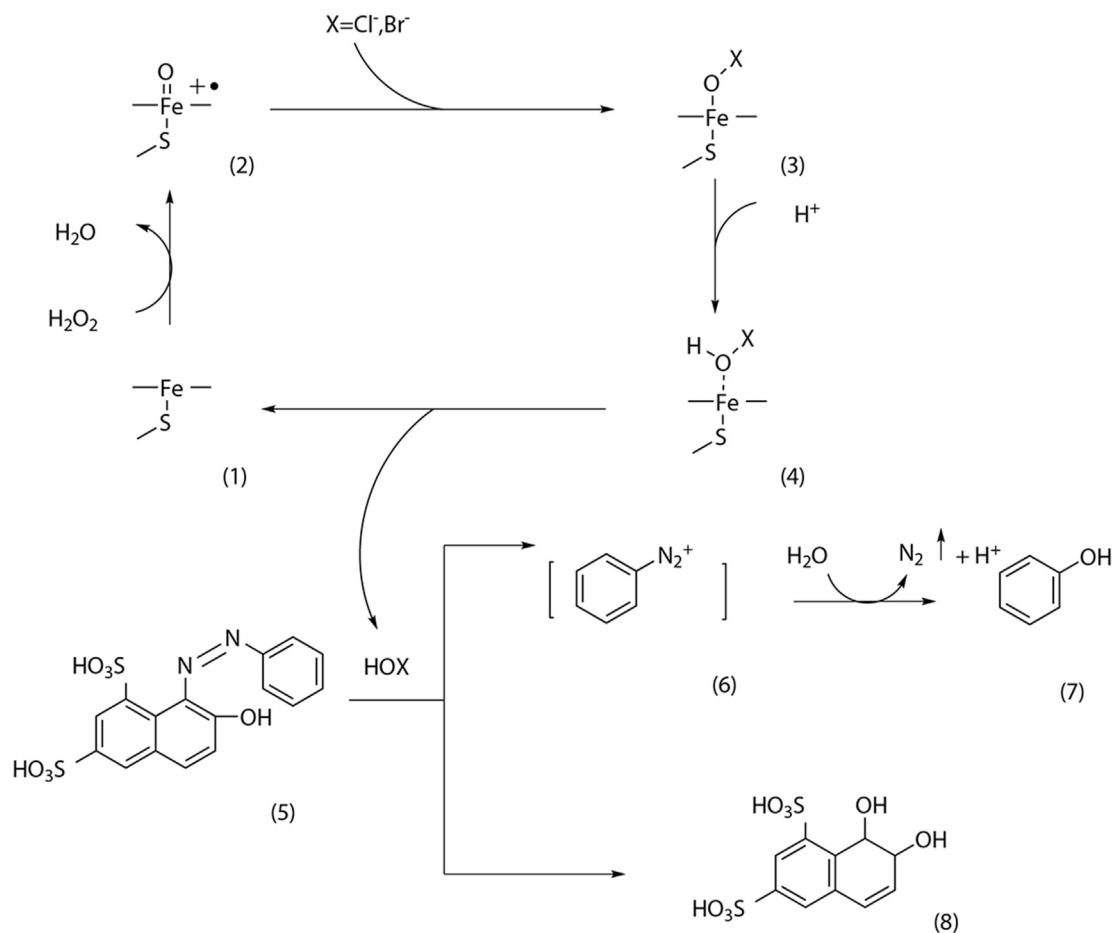


Fig. 6. Proposed mechanism of orange G degradation (X = Cl<sup>-</sup> or Br<sup>-</sup>).

#### 4. Conclusion

In summary, we have demonstrated the imperative role of halide ion played in CPO catalyzed degradation of orange G although no halogenated products are identified. Our results suggest the formation of compound X, a hypochlorite-heme adduct intermediate during CPO-catalyzed orange G degradation. The structural feature of compound X revealed by our QM/MM studies suggested a synergistic action between Glu 183 and His 105 in the formation of HClO and regeneration of the resting state CPO. Our work demonstrates that CPO-catalyzed halide-dependent degradation of orange G is strictly regioselective with the cleavage exclusively at naphthalene carbon-nitrogen bond. This study also provides evidence about the general chlorination mechanisms, which has promising potential in environmental applications [85,86].

#### Acknowledgements

This work is supported by the National Science Foundation via Grant CHE-0540763 to X.W. (CAREER Award), and a start-up fund from Florida International University. The authors wish to acknowledge FIU's NMR facility for the use of its Bruker Avance 600 MHz spectrometer sponsored by a grant from DOE.

#### Appendix. ASupplementary data

Supplementary data related to this article can be found at <http://>

[dx.doi.org/10.1016/j.abb.2016.02.026](http://dx.doi.org/10.1016/j.abb.2016.02.026).

#### References

- [1] D.R. Morris, L.P. Hager, *J. Biol. Chem.* 241 (1966) 1763–1768.
- [2] J.A. Thomas, D.R. Morris, L.P. Hager, *J. Biol. Chem.* 245 (1970) 3129–3134.
- [3] S. Kobayashi, M. Nakano, T. Goto, T. Kimura, A.P. Schaap, *Biochem. Biophys. Res. Commun.* 135 (1986) 166–171.
- [4] S. Colonna, N. Gaggero, A. Manfredi, L. Casella, M. Gullotti, G. Carrea, P. Pasta, *Biochemistry* 29 (1990) 10465–10468.
- [5] J. Geigert, D.J. Dalietos, S.L. Neidleman, T.D. Lee, J. Wadsworth, *Biochem. Biophys. Res. Commun.* 114 (1983) 1104–1108.
- [6] M.D. Corbett, D.G. Baden, B.R. Chipko, *Bioorg. Chem.* 8 (1979) 91–95.
- [7] S.H. Hu, L.P. Hager, *Biochem. Biophys. Res. Commun.* 253 (1998) 544–546.
- [8] A. Zaks, D.R. Dodds, *J. Am. Chem. Soc.* 117 (1995) 10419–10424.
- [9] S.H. Hu, L.P. Hager, *J. Am. Chem. Soc.* 121 (1999) 872–873.
- [10] R.L. Osborne, G.M. Raner, L.P. Hager, J.H. Dawson, *J. Am. Chem. Soc.* 128 (2006) 1036–1037.
- [11] R. Chiang, T. Rand-Meir, R. Makino, L.P. Hager, *J. Biol. Chem.* 251 (1976) 6340–6346.
- [12] J.H. Dawson, M. Sono, *Chem. Rev. Wash. D.C. U. S.* 87 (1987) 1255–1276.
- [13] J.H. Dawson, *Science* 240 (1988) 433–439.
- [14] R.D. Libby, T.M. Beachy, A.K. Phipps, *J. Biol. Chem.* 271 (1996) 21820–21827.
- [15] G.P. Rai, S. Sakai, A.M. Florez, L. Mogollon, L.P. Hager, *Adv. Synth. Catal.* 343 (2001) 638–645.
- [16] P. Pasta, G. Carrea, S. Colonna, N. Gaggero, *Biochim. Biophys. Acta* 1209 (1994) 203–208.
- [17] J. Zhang, M. Feng, Y. Jiang, M. Hu, S. Li, Q. Zhai, *Chem. Eng. J. Amst. Neth.* 191 (2012) 236–242.
- [18] A. Bafana, S.S. Devi, T. Chakrabarti, *Environ. Rev. Ott. Can.* 19 (2011) 350–371.
- [19] Q. Husain, *Rev. Environ. Sci. Biotechnol.* 9 (2010) 117–140.
- [20] A. Stolz, *Appl. Microbiol. Biotechnol.* 56 (2001) 69–80.
- [21] H. Zollinger, *Color Chemistry: Syntheses, Properties, and Applications of Organic Dyes and Pigments*, VCH, New York, NY, 2004.
- [22] U. Pagga, D. Brown, *Chemosphere* 15 (1986) 479–491.
- [23] H.G. Kulla, F. Klausener, U. Meyer, B. Lüdeke, T. Leisinger, *Arch. Microbiol.* 135

- (1983) 1–7.
- [24] E. Forgacs, T. Cserhati, G. Oros, *Environ. Int.* 30 (2004) 953–971.
- [25] R.G. Saratale, G.D. Saratale, J.S. Chang, S.P. Govindwar, *J. Taiwan Inst. Chem. Eng.* 42 (2011) 138–157.
- [26] H. Chen, *Curr. Protein. Pept. Sci.* 7 (2006) 101–111.
- [27] M.A. Pickard, T.A. Kadima, R.D. Carmichael, *J. Ind. Microbiol. Biotechnol.* 7 (1991) 235–241.
- [28] R.L. Osborne, G.M. Raner, L.P. Hager, J.H. Dawson, *J. Am. Chem. Soc.* 128 (2006) 1036–1037.
- [29] S.R. Blanke, S. Yi, L.P. Hager, *Biotechnol. Lett.* 11 (1989) 769–774.
- [30] P.F. Hallenberg, L.P. Hager, *Methods Enzymol.* 52 (1978) 521–529.
- [31] A. Hashimoto, M.A. Pickard, *J. Gen. Microbiol.* 130 (1984) 2051–2058.
- [32] S. Blumel, H.J. Knackmuss, A. Stolz, *Appl. Environ. Microbiol.* 68 (2002) 3948–3955.
- [33] F. Delaglio, S. Grzesiek, G.W. Vuister, G. Zhu, J. Pfeifer, A. Bax, *J. Biomol. NMR* 6 (1995) 277–293.
- [34] M. Valiev, E.J. Bylaska, N. Govind, K. Kowalski, T.P. Straatsma, H.J.J. Van Dam, D. Wang, J. Nieplocha, E. Apra, T.L. Windus, W. de Jong, *Comput. Phys. Commun.* 181 (2010) 1477–1489.
- [35] K.B. Cho, H. Hirao, H. Chen, M.A. Carvajal, S. Cohen, E. Derat, W. Thiel, S. Shaik, *J. Phys. Chem. A* 112 (2008) 13128–13138.
- [36] A.D. Becke, *J. Chem. Phys.* 98 (1993) 5648–5652.
- [37] P.J. Stephens, F.J. Devlin, C.F. Chabalowski, M.J. Frisch, *J. Phys. Chem.* 98 (1994) 11623–11627.
- [38] P.J. Hay, W.R. Wadt, *J. Chem. Phys.* 82 (1985) 299–310.
- [39] M.M. Francl, W.J. Pietro, W.J. Hehre, J.S. Binkley, M.S. Gordon, D.J. Defrees, J.A. Pople, *J. Chem. Phys.* 77 (1982) 3654–3665.
- [40] W.D. Cornell, P. Cieplak, C.I. Bayly, I.R. Gould, K.M. Merz, D.M. Ferguson, D.C. Spellmeyer, T. Fox, J.W. Caldwell, P.A. Kollman, *J. Am. Chem. Soc.* 117 (1995) 5179–5197.
- [41] G. Henkelman, H. Jonsson, *J. Chem. Phys.* 113 (2000) 9978–9985.
- [42] G.M. Morris, D.S. Goodsell, R.S. Halliday, R. Huey, W.E. Hart, R.K. Belew, A.J. Olson, *J. Comput. Chem.* 19 (1998) 1639–1662.
- [43] R. Zhang, Q. He, D. Chatfield, X. Wang, *Biochemistry* 52 (2013) 3688–3701.
- [44] F. Neese, *Wiley Interdiscip. Reviews-Computational Mol. Sci.* 2 (2012) 73–78.
- [45] M.F. Sanner, *J. Mol. Graph. Modell.* 17 (1999) 57–61.
- [46] S.J. Zhang, H.Q. Yu, Y. Zhao, *Water. Res.* 39 (2005) 839–846.
- [47] W. Feng, D. Nansheng, H. Helin, *Chemosphere* 41 (2000) 1233–1238.
- [48] J.E. Harrison, J. Schultz, *J. Biol. Chem.* 251 (1976) 1371–1374.
- [49] A.J. Kettle, C.C. Winterbourn, *Biochem. J.* 263 (1989) 823–828.
- [50] R. Senthilmohan, A.J. Kettle, *Arch. Biochem. Biophys.* 445 (2006) 235–244.
- [51] R.D. Libby, J.A. Thomas, L.W. Kaiser, L.P. Hager, *J. Biol. Chem.* 257 (1982) 5030–5037.
- [52] A. Butler, M. Sandy, *Nature* 460 (2009) 848–854.
- [53] L.P. Hager, D.R. Morris, F.S. Brown, H. Eberwein, *J. Biol. Chem.* 241 (1966) 1769–1777.
- [54] M. Sono, J.H. Dawson, K. Hall, L.P. Hager, *Biochemistry* 25 (1986) 347–356.
- [55] M. Sundaramoorthy, J. Terner, T.L. Poulos, *Struct. Camb. MA, U. S. 3* (1995) 1367–1378.
- [56] K. Kuhnel, W. Blankenfeldt, J. Terner, I. Schlichting, *J. Biol. Chem.* 281 (2006) 23990–23998.
- [57] A.M. Lambeir, H.B. Dunford, *J. Biol. Chem.* 258 (1983) 13558–13563.
- [58] H.A. Wagenknecht, W.D. Woggon, *Chem. Biol.* 4 (1997) 367–372.
- [59] J.A. Thomas, D.R. Morris, L.P. Hager, *J. Biol. Chem.* 245 (1970) 3135–3142.
- [60] R.D. Libby, A.L. Shedd, A.K. Phipps, T.M. Beachy, S.M. Gerstberger, *J. Biol. Chem.* 267 (1992) 1769–1775.
- [61] K.M. Manoj, A. Baburaj, B. Ephraim, F. Pappachan, P.P. Maviliparambathu, U.K. Vijayan, S.V. Narayanan, K. Periasamy, E.A. George, L.T. Mathew, *PLoS One* 5 (2010) e10601.
- [62] M. Ayala, C.V. Batista, R. Vazquez-Duhalt, *J. Biol. Inorg. Chem.* 16 (2011) 63–68.
- [63] B. Valderrama, R. Vazquez-Duhalt, *J. Mol. Catal. B Enzym* 35 (2005) 41–44.
- [64] H. Kanazawa, T. Onami, *Color. Technol.* 117 (2006) 323–327.
- [65] E.A. Moelwyn-Hughes, P. Johnson, *Trans. Faraday Soc.* 36 (1940) 0948–0955.
- [66] J. Madhavan, F. Grieser, M. Ashokkumar, *Ultraso. Sonochem* 17 (2010) 338–343.
- [67] E. Argese, C. Bettiol, G. Giurin, P. Miana, *Chemosphere* 38 (1999) 2281–2292.
- [68] J. Huff, *Chemosphere* 89 (2012) 521–525.
- [69] C. D’Cunha, A.N. Morozov, D.C. Chatfield, *J. Phys. Chem. A* 117 (2013) 8437–8448.
- [70] H.B. Dunford, A.M. Lambeir, M.A. Kashem, M. Pickard, *Arch. Biochem. Biophys.* 252 (1987) 292–302.
- [71] H. Chen, J.S. Song, W.Z. Lai, W. Wu, S. Shaik, *J. Chem. Theory Comput.* 6 (2010) 940–953.
- [72] K.L. Stone, R.K. Behan, M.T. Green, *Proc. Natl. Acad. Sci. U. S. A.* 102 (2005) 16563–16565.
- [73] W.Z. Lai, H. Chen, S. Shaik, *J. Phys. Chem. B* 113 (2009) 7912–7917.
- [74] M.T. Green, J.H. Dawson, H.B. Gray, *Science* 304 (2004) 1653–1656.
- [75] A.N. Morozov, D.C. Chatfield, *J. Phys. Chem. B* 116 (2012) 12905–12914.
- [76] A.N. Morozov, C. D’Cunha, C.A. Alvarez, D.C. Chatfield, *Biophys. J.* 100 (2011) 1066–1075.
- [77] X. Yi, A. Conesa, P.J. Punt, L.P. Hager, *J. Biol. Chem.* 278 (2003) 13855–13859.
- [78] R. Rutter, L.P. Hager, H. Dhonau, M. Hendrich, M. Valentine, P. Debrunner, *Biochemistry* 23 (1984) 6809–6816.
- [79] H. Chen, H. Hirao, E. Derat, I. Schlichting, S. Shaik, *J. Phys. Chem. B* 112 (2008) 9490–9500.
- [80] F.H. Vaillancourt, E. Yeh, D.A. Vosburg, S. Garneau-Tsodikova, C.T. Walsh, *Chem. Rev. Wash. D.C. U. S.* 106 (2006) 3364–3378.
- [81] C.G. Swain, A.D. Ketley, *J. Am. Chem. Soc.* 77 (1955), 3410–3410.
- [82] C.G. Swain, D.R. Crist, *J. Am. Chem. Soc.* 94 (1972) 3195–3200.
- [83] H. Spalteholz, K. Wenske, O.M. Panasenka, J. Schiller, J. Arnhold, *Chem. Phys. Lipids* 129 (2004) 85–96.
- [84] T. Cohen, A.G. Dietz, J.R. Miser, *J. Org. Chem.* 42 (1977) 2053–2058.
- [85] L. Getrey, T. Krieg, F. Hollmann, J. Schrader, D. Holtmann, *Green Chem.* 16 (2014) 1104–1108.
- [86] F. Breider, D. Hunkeler, *Environ. Sci. Technol.* 48 (2014) 1592–1600.